Disease-Induced Alterations in Brain Drug Transporters in Animal Models of Alzheimer's Disease

Kati-Sisko Vellonen, Jouni Ihalainen, Marie-Christine Boucau, Fabien Gosselet, Théo Picardat, Mikko Gynther, Katja Kanninen, Anthony White, Tarja Malm, Jari Koistinaho, et al.

Pharm Res (2017) 34:2652–2662
DOI 10.1007/s11095-017-2263-7

RESEARCH PAPER

Disease-Induced Alterations in Brain Drug Transporters in Animal Models of Alzheimer's Disease

Theme: Drug Discovery, Development and Delivery in Alzheimer's Disease
Guest Editor: Davide Brambilla

Kati-Sisko Vellonen[1] • Jouni Ihalainen[1] • Marie-Christine Boucau[2] • Fabien Gosselet[2] • Théo Picardat[1] • Mikko Gynther[1] • Katja M. Kanninen[3] • Anthony R. White[4] • Tarja Malm[3] • Jari Koistinaho[3] • Markus M. Forsberg[1] • Marika Ruponen[1]

Received: 20 June 2017 / Accepted: 12 September 2017 / Published online: 26 September 2017

ABSTRACT

Purpose Alzheimer's disease (AD) may disturb functions of the blood-brain barrier and change the disposition of drugs to the brain. This study assessed the disease-induced changes in drug transporters in the brain capillaries of transgenic AD mice.

Methods Eighteen drug transporters and four tight junction-associated proteins were analyzed by RT-qPCR in cortex, hippocampus and cerebellum tissue samples of 12–16-month-old APdE9, Tg2576 and APP/PS1 transgenic mice and their healthy age-matched controls. In addition, microvessel fractions enriched from 1-3-month-old APdE9 mice were analyzed using RT-qPCR and Western blotting. Brain transport of methotrexate in APdE9 mice was assessed by in vivo microdialysis.

Results The expression profiles of studied genes were similar in brain tissues of AD and control mice. Instead, in the microvessel fraction in APdE9 mice, >2-fold alterations were detected in the expressions of 11 genes but none at the protein level. In control mice strains, >5-fold changes between different brain regions were identified for Slc15a2, Slc22a3 and occludin. Methotrexate distribution into hippocampus of APdE9 mice was faster than in controls.

Conclusions The expression profile of mice carrying presenilin and amyloid precursor protein mutations is comparable to controls, but clear regional differences exist in the expression of drug transporters in brain.

KEY WORDS APdE9 · blood-brain barrier · brain disposition · brain microdialysis · CNS exposure · pharmacokinetics

ABBREVIATIONS

AD	Alzheimer's disease
amyloid-β	Aβ
BBB	Blood-brain barrier
CB	Cerebellum
CX	Cortex
HC	Hippocampus
wt	Wild type

INTRODUCTION

Alzheimer's disease (AD) is the most common form of dementia; it is associated with accumulation of senile plaques and neurofibrillary tangles in the brain (1). The extracellular senile plaques are mainly formed by aggregating amyloid-β (Aβ) peptides in the brain parenchyma, whereas hyperphosphorylated and misfolded tau proteins are the main constituent of the intraneuronal neurofibrillary tangles.

The distribution of drug molecules from the systemic circulation to the brain is controlled and limited by the blood-brain barrier (BBB). The BBB is formed by capillary endothelial cells and supported by the end feet of astrocytes and pericytes around brain capillaries. Dysfunction of the BBB has been

Electronic supplementary material The online version of this article (https://doi.org/10.1007/s11095-017-2263-7) contains supplementary material, which is available to authorized users.

✉ Kati-Sisko Vellonen
Kati-Sisko.Vellonen@uef.fi

[1] School of Pharmacy, University of Eastern Finland, P.O. Box 1627, 70211 Kuopio, FI, Finland

[2] Laboratoire de la barrière hémato-encéphalique (LBHE), University Artois, Lens, France

[3] A. I. Virtanen Institute for Molecular Sciences, University of Eastern Finland, Kuopio, Finland

[4] QIMR Berghofer Medical Research Institute, Herston, QLD, Australia

associated with neurodegeneration, although the importance of BBB alterations solely attributable to AD, without the presence of additional vascular diseases, is still unclear (2). A dysfunctional BBB may alter the access of AD drugs to their site of action; it may either increase the drug exposure to the brain, potentially causing unwanted effects, or decrease drug access and lead to an insufficient response. AD patients are generally over 65 years old, and in addition to AD drugs, they often have medication for several other chronic diseases. Therefore, BBB dysfunction can also either increase or decrease the brain distribution of other concomitant medications and possibly increase their adverse effects on the central nervous system.

The BBB is enriched with several transporter proteins belonging to the ATP binding cassette (ABC) and solute carrier (SLC) gene families; these are responsible for ensuring the supply of dietary components into the brain and the disposal of metabolic products from the brain, as well as preventing noxious agents accessing the brain from the circulation (3). Transporters have also a significant role in the pharmacokinetics of many drugs. For instance, L-dopa, which is used to treat Parkinson's disease, crosses the BBB via the influx carrier L-type amino acid transporter (LAT1). Furthermore, the efflux transporter Multidrug resistance protein 1 (MDR1, P-glycoprotein) is known to diminish the central access of various drug molecules. In addition, high levels of efflux transporters including Breast cancer resistance protein (BCRP, *ABCG2*) and Multidrug resistance-associated protein 4 (MRP4, *ABCC4*) are expressed by the endothelial cells in the BBB (4). Other transporters, relevant also as drug carriers, such as MRP proteins (MRP1, MRP5), monocarboxylate (MCT1), nucleoside (ENT1) and organic cation (OCT3) and anion (OAT3) transporters, organic anion transporting polypeptides (OATPs) and multidrug and toxin extrusion protein 1 (MATE1) have been localized in the endothelial cells of human and mouse brain capillaries (3–7).

The influence of AD on the expression and functionality of some BBB drug transporters has been studied both in post-mortem AD patient samples and animal models of AD. MDR1 has been the most widely studied efflux protein in AD and in addition to a wide variety of drug molecules it has been shown to also transport Aβ (8). Downregulation of MDR1 expression in brain capillaries in close proximity to Aβ deposits of AD patients has been observed by several groups (9–13). In addition to expression, a positron emission tomography study investigated MDR1 function in the BBB of AD patients with MDR1 substrate (R)-[^{11}C]verapamil and found evidence of decreased efflux function (14). The findings related to the impact of AD on BCRP expression have revealed minor and also partly conflicting alterations (10,12,13,15) and a slight upregulation of MRP4 expression at both RNA and protein levels has been detected in the hippocampus of AD patients (10). There are even fewer studies examining disease-induced changes in drug transporter expression in AD mouse models. With respect to Mdr1, both up- and down-regulation have been reported, whereas increase in expression levels of Bcrp have been detected (8,16,17). However, there are many transporters whose expression and functionality in AD remain obscure i.e. no comprehensive comparative data is available.

Transgenic mouse models of AD, which have mutations in amyloid precursor protein (APP), such as Tg2576, or in both APP and presenilin (PSEN1) genes, such as APdE9 and APP/PS1 mouse models, can provide useful information on AD pathogenesis and disease mechanisms. APdE9 mice exhibit an increase in the parenchymal Aβ load, with the appearance of Aβ plaques starting from the age of four months; APP/PS1 mice develop Aß deposits around 9 months of age, and Tg2576 mice around 10 months of age. In addition, signs of gliosis can be seen concurrently. Disease models are important tools for drug development. For example, the pharmacokinetic properties of novel AD drug candidates can be studied in models having similar disease-induced alterations as AD patients. Before these AD models can be better exploited in preclinical drug development, it would be important to acquire a more detailed characterization of the drug transporters.

This study aimed to characterize the expression of drug transporters and tight junction-associated proteins in three mouse models of AD, the APdE9, APP/PS1 and Tg2576 mice, and to investigate the regional expression differences in the brain. In order to assess the effect of AD pathology on drug transport into the brain in vivo, we applied a pharmacokinetic microdialysis method to measure the unbound extracellular drug levels in the hippocampus after systemic administration of methotrexate.

MATERIALS AND METHODS

Animals

All procedures were made in compliance with the European Communities Council Directive (86/609/EEC) and Principles of laboratory Animal Care, and studies were approved by the National Animal Experiment Board. The animals were kept in a controlled environment with 12 h light/dark cycle and food and water freely available. Brain tissue samples were collected from male APP/PS1dE9 (APdE9) mice (C57BL/6 J strain) (18) at the age of 16 months (n = 3–4), female APP/PS1 mice (C57BL/6 J strain) (19) at the age of 12–15 months (n = 3–4) and female Tg2576 mice (C57BL/6JxSJL strain) (20) at the age of 12–15 months (n = 4). All mice groups had age-matched wildtype (wt) controls (n = 3–5). During sample collection, the mice were anesthetized with 250 mg/kg Avertin and perfused 3 min transcardially with heparinized (2500 IU/l) saline at a flow rate of 20 ml/min. The cortical (CX), hippocampal (HC) and cerebellar (CB) samples were dissected and snap frozen in liquid nitrogen.

Aβ accumulates mainly in CX and HC, whereas CB remains devoid of Ab deposits and was therefore considered as unaffected control tissue.

Mechanical Isolation of Brain Capillaries

The microvessel enriched fraction was isolated from 5–12 weeks old female APdE9 mice as previously described by Coisne *et al.* (21). Briefly, ten cortices, from APdE9 or wt mice were isolated by removing cerebellum and brain white matter. Outer vessels and meninges were also removed. Preparations were pooled and ground using a Dounce homogenizer (first with the loose clearance pestle: 25–80 μm, then with the tight clearance pestle: 5–25 μm) in HBSS 1x containing 10 mM HEPES and 0.1% BSA. The resulting homogenate was mixed with 30% dextran (*v*/v, molecular weight 100,000–200,000) in HBSS 1x supplemented with 10 mM HEPES and 0.1% BSA. This suspension was centrifuged at 3000 g for 25 min at 4°C. The neural component and the dextran layer were discarded and the pellet containing the vascular component was washed twice in cold PBS CMF and then separated into two equal parts by centrifugation at 1000 g for 7 min at 4°C. The resulting pellets were resuspended either in RLT lysis buffer for RNA extraction or in RIPA lysis buffer for protein extraction.

Quantitative RT-PCR

RNA expression of drug transporter and tight junction-associated genes was studied in brain tissues of 12–16 months old mice modelling AD and their healthy age-matched controls. Total RNA was extracted from HC, CX and CB tissue samples with TRI Reagent (Sigma). From microvessel samples, the RNA was extracted by RNeasy Mini Kit (Qiagen). After RNA extraction, the procedure was similar for both tissue and microvessel samples. Possible DNA residues were removed with DNA-free™ kit (Ambion). RNA concentration was measured with Nanodrop 1000 (Thermo Fisher Scientific) or NanoVue (GE Healthcare) spectrophotometer and 500 ng (brain tissues) or 200 ng (microvessels) of RNA was reverse-transcribed using random primers and M-MuLV enzyme (Fermentas, Hanover, MD). In the quantitative real-time PCR, the ABI Prism 7500 instrument with TaqMan® Gene expression assays (Supplementary Table I) or SYBR Green chemistry and primers designed for each gene (Supplementary Table II) were used. Normalized expression was calculated with the QGene application (22) using beta-actin as the reference gene. In the microvessel enriched fraction, a 2-fold difference was used as a threshold value and when a > 2-fold difference was determined with the first batch, the results were confirmed with a second batch. Efficiency was calculated for each primer pair and a melting curve analysis was performed after amplification cycles, in order to check the specificity/purity of each amplification.

Western Blotting

After the capillary isolation procedure, the pellet was washed twice with cold PBS-CMF and then homogenized (polytron homogeniser: 2 times for 15 s at 11000 r/min on ice) in cold RIPA lysis buffer (Millipore, containing 0.5 M Tris-HCl, pH 7.4, 1.5 M NaCl, 2.5% deoxycholic acid, 10% NP-40 and 10 mM EDTA, supplemented with phosphatase and protease inhibitor cocktails (Sigma-Aldrich)). The protein concentration in each sample was determined by the method of Bradford (Bio-Rad). Then, 5–40 μg of proteins were electrophoresed on 4–15% Criterion XT sodium dodecyl sulphate (SDS)-polyacrylamide gel (P-gp/Abcb1, Rage, Lrp1) or 4–20% Mini-Protean TGX Gel (Mrp4) (Bio-Rad) and subsequently electrotransferred to nitrocellulose membranes. Unspecific binding was blocked with 5% skimmed milk in TBS, 0.1% Tween 20 and then incubated with primary antibody using following dilutions: Rage (Abcam) 1:2000, P-gp/Abcb1 (C219) (Genetex) 1:400, Lrp (5A6) (Santa Cruz) 1:200, Mrp4 (M41–10) (Santa Cruz) 1:200, β-actin (AC-15) (Sigma-Aldrich) 1:20,000, α-tubulin (B-5-1-2) (Sigma-Aldrich) 1:8000 and β-tubulin (9F3) (Cell Signaling) 1:1000. Immunoreactivity was detected with HRP conjugated secondary antibodies (Goat anti-rat IgG (Santa Cruz) (1: 10,000), Goat anti-rabbit IgG (Dako) (1:2000) and Goat anti-mouse IgG (1:2000 for Dako and 1:7500 for Santa Cruz) and enhanced chemiluminescence (ECL) system.

Pharmacokinetic *In Vivo* Microdialysis

Microdialysis experiments were performed with 16–18 months old male APdE9 mice. To implant the guide cannulae (Brainlink B.V., the Netherlands) 2–3 days before the microdialysis experiment, the mice were anesthetized with 1–2% isoflurane in 70% N_2O and 30% O_2 (flow 300 ml/min, induction 5% isoflurane). Lidocaine (10 mg/mL; Orion Corporation, Oulu, Finland) was used as a local anesthetic. Anesthetized mice were placed in a Kopf stereotaxic frame equipped with a DKI 921 mouse adapter (David Kopf Instr., Tujunga, CA, USA). The guide cannula was implanted into the right HC using following coordinates: A: −3.1 mm, L: −2.7 mm, V: −1.3 mm and secured with cranial screws and dental cement. Carprofen (5 mg/kg s.c.; Vericore Ltd., Dundee, UK) and buprenorphine (0.12 mg/kg, s.c.; Schering-Plough, Belgium) were used for post-operative pain relief. Saline (0.6 mL i.p.) was injected after surgery to maintain fluid balance.

Three hours before the start of the microdialysis experiment, the mice were transferred into microdialysis bowls (CMA120, CMA microdialysis, Solna, Sweden), and the microdialysis probe (membrane length 3 mm, regenerated cellulose; cut-off 18 kDa; Brainlink B.V., the Netherlands) was inserted into the right HC through the guide cannula. The probe was connected to a rotating liquid swivel (375/D/

22QM, Instech Laboratories, Plymouth Meeting, PA, USA) and was perfused with Ringer fluid (147 mM NaCl, 3 mM KCl, 1.2 mM $CaCl_2$, 1.2 mM $MgCl_2$) at a flow rate of 1.5 μl/min. After a 120-min wash-out period, a 20 min baseline sample was collected and methotrexate (50 mg/kg in a volume of 2.5 ml/kg; Metoject, medac GmbH) was given intravenously. Dialysate was collected for 240 min (12 samples), and the samples were frozen in liquid nitrogen and stored at −70°C. Terminal blood samples were collected by cardiac puncture and plasma was separated by centrifugation (2000 × g for 10 min at 4°C), immediately fresh frozen on liquid nitrogen and stored at −70°C.

In vivo recovery was determined to estimate the true methotrexate concentration in the brain extracellular fluid in a separate experiment (wt $n = 3$ and APdE9 n = 3, 13 months) by using the retrodialysis method to calibrate the microdialysis probe. The basic procedure of *in vivo* microdialysis was performed as described above. After a 120-min wash-out period, a 20 min baseline sample was collected and then the Ringer solution was switched to a Ringer containing 200 ng/mL methotrexate. The microdialysis sample collection was continued for 120 min (6 samples). The *in vivo* recovery for methotrexate was calculated from the last three samples with the eq. C = (Cin-Cout)/Cin, where R is *in vivo* recovery of methotrexate, Cin is concentration of methotrexate in the perfusate and Cout is concentration of methotrexate in the dialysate. *In vivo* recovery values of 8 ± 3% for APdE9 mice and 18 ± 7% for WT mice were used to correct the dialysate concentrations.

LC-MS/MS Analysis

The microdialysis samples were analyzed for MTX concentration with an Agilent 1200 series liquid chromatograph and an Agilent 6410 Triple Quadrupole Mass Spectrometer with electrospray ionization. The column was a Poroshell 120 EC-C18 (50 mm × 2.1 mm, 2.7 μm; Agilent Technologies, Santa Clara, CA) maintained at 40°C and a Rapid Resolution LC in-line filter (2 mm, 0.2 mm; Agilent Technologies) was used for protecting the analytical column from possible contaminants. A binary mobile phase with a gradient elution was used. Solvent A was milliQ water with 0.1% formic acid (eluent additive for LC-MS, Fluka) and solvent B was acetonitrile (Sigma-Aldrich) with 0.1% formic acid. The gradient was performed as following: 5% B kept constant for 1 min, increased to 90% for 5 min, decreased to 5% B for 0.1 min, and kept constant for 2.9 min. Under these conditions, the total run time was 8 min. The flow rate was 0.3 ml/min and the injection volume of Ringer fluid samples was 20 μl. The source parameters were: capillary voltage 3 kV, nebuliser 40 psi, gas temperature 300°C, gas flow 8 l/min. Data acquisition was done in the positive ion MRM mode using transitions 455.1 → 308 for MTX and 458.1 → 311 for the internal standard (deuterated MTX). Fragmentor voltages used for MTX and the internal standard were 200 V and 160 V, respectively. The collision energies were 38 V and 16 V for MTX and the internal standard, respectively. Agilent MassHunter Workstation Acquisition software (Data Acquisition for Triple Quadrupole Mass Spectrometer, version B.03.01) was used for data acquisition, whereas Quantitative Analysis (B.04.00) software was used for the data processing and analysis. The lower limit of quantification (LLOQ) was 0.05 ng/ml for Ringer fluid samples and 5 ng/ml for plasma samples. The linearity of the calibration curve was evaluated by a quadratic regression analysis and the method was found to be selective, accurate, and precise over the calibration range. The calibration range of 0.05–500 ng/ml was used for Ringer fluid samples and 5–1000 ng/ml for plasma samples. Within-run accuracy and precision were calculated from the results of the quality control samples at the three concentrations. The accuracies and precisions for quality control concentrations of 20% were considered acceptable.

Data Analysis

To evaluate differences in gene expression between brain tissues the statistical significance was tested with Kruskal-Wallis one way analysis of variance on Ranks followed by Dunn's Method for pairwise comparison (SigmaPlot 13.0).

The area under the concentration curve (AUC) values were determined using Phoenix™ WinNonlin® (Pharsight, Certara L.P., USA). In the statistical analysis of differences between AUC values, two-tailed t-test (SigmaPlot 13.0) was used.

RESULTS

Gene Expression Profile of Drug Transporters and Tight Junction-Associated Proteins in Brain of AD Mouse Models

Efflux Transporters

The expressions of 8 ABC efflux transporters (Abcb1a, Abcb1b, Abcc1-Abcc5, Abcg2) were compared between AD mouse models APdE9, Tg2576 and APP/PS1 (12–16 months old mice) and their healthy age-matched wt controls using brain samples comprising of brain parenchyma and BBB. In the APdE9 model, the greatest difference was detected for Abcb1b gene, which had a 1.4-fold higher expression level in AD CX and HC tissues when compared to wt (Fig. 1a). In Tg2576 mice, the differences between AD tissues and controls were ≤1.4-fold (Fig. 1b) and in the APP/PS1 model, the differences were even smaller (≤ 1.3-fold) (Fig. 1c), if Abcc2 was not taken into account. With respect to Abcc2, up to 2-fold differences were detected, but statistical significance was not reached because of the high variation in Abcc2 expression

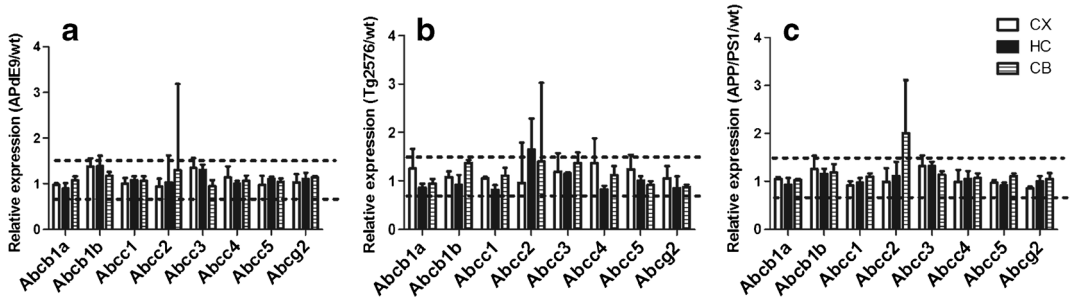

Fig. 1 Gene expression of Abc efflux transporters in the CX, HC and CB of male APdE9 (**a**), female Tg2576 (**b**) and female APP/PS1 (**c**) mouse models expressed as relative to wt control mice (AD/wt) (mean ± sd, $n = 3–5$). The gene expression was normalized against the beta-actin house-keeping gene. The dotted line depicts 1.5-fold down- or up-regulation.

due to its very low expression levels. Overall, the gene expression profile of efflux transporters between these three AD models was similar. Differences between AD and wt were minor (≤ 1.4 fold) with the exception of Abcc2.

Influx Transporters

Gene expression of SLC influx transporters including L-type amino acid transporter (Slc7a5), peptide transporter (Slc15a2), organic anion and cation transporters (Slc22a2, Slc22a3, Slc22a5 and Slc22a8), Multidrug and toxin extrusion protein (Slc47a1) and organic anion transporting polypeptides (Slco1a4, Slco2b1 and Slco1c1) was studied in the three AD mouse models (Fig. 2). More than 2-fold lower expression in AD samples compared to wt controls was observed for four transporters, namely Slc22a2 (HC of APdE9 and Tg2576), Slc22a3 (CB of Tg2576), Slc22a8 (HC of Tg2576) and Slc47a1 (HC of APdE9 and Tg2576). The highest difference was seen for Slc22a2, the expression of which in HC of Tg2576 mice was approximately one fifth of that in control and a similar trend was also seen in APdE9 (less than half than in controls). The Slc22a8 expression level in the HC of Tg2576 mice was one third of the control and similarly in APdE9, almost half of the control. In APP/PS1 brains, the differences between AD and control were in all cases <1.5 fold. Slc22a2 was expressed at a low level in all studied brain samples; likewise, the levels of Slc22a3 and Slc47a1 were low in certain tissues, thereby introducing high variability into the results for those genes.

Tight Junction-Associated Proteins and Cell Markers

Four genes (Ocln, Cldn3, Cldn5, Jam1) related to tight junctions were included in the study. Cldn3 expression in HC of Tg2576 and APdE9 mice was lower (0.43 ± 0.14 and 0.61 ± 0.30, respectively) compared to wt control and similarly Jam1 in HC of Tg2576 (0.61 ± 0.11), but in other brain regions and animal models, the differences were smaller (Fig. 3). For the other tight junction-associated genes (Ocln, Cldn5), only minor differences were seen between AD and wt controls. However, with regard to the cell markers analyzed (Pecam1, Aif1, Rbfox3, Gfap), a clear upregulation of the astrocyte marker Gfap was detected. In the CX of APdE9, Tg2576 and APP/PS1 mice, the expression of Gfap was 3.5 ± 0.2-fold ($p = 0.037$), 2.27 ± 1.13-fold and 4.4 ± 0.2-fold ($p = 0.029$) higher, respectively, than in wt controls. In addition, in HC, the AD/wt ratio was elevated, i.e. it was 2.4 ± 0.4 in APP/PS1 and 2.3 ± 0.2 in APdE9. The microglial marker Aif1 expression was upregulated only in APdE9 mice, with 1.6-fold and 1.5-fold higher expressions in HC and CX, respectively.

When the expression levels of 26 genes were compared between brain regions (CX, HC and CB) of wt control mice, the differences were more prominent (Table I) and more than

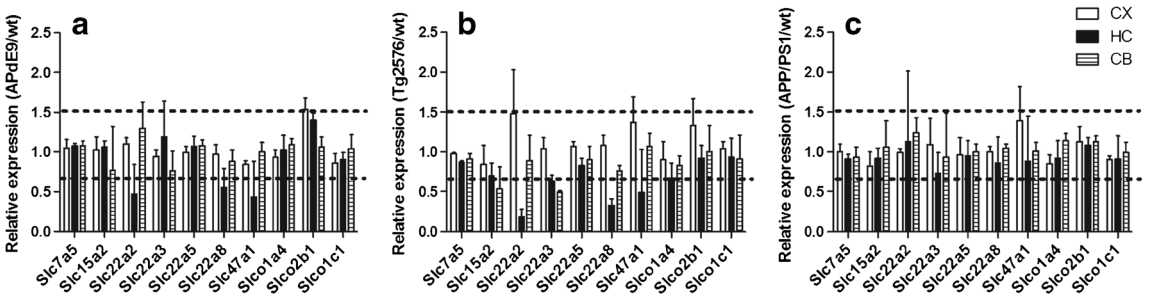

Fig. 2 Gene expression of Slc influx transporters in the CX, HC and CB of male APdE9 (**a**), female Tg2576 (**b**) and female APP/PS1 (**c**) mouse models expressed as relative to wt control mice (AD/wt) (mean ± sd, n = 3–5). The gene expression was normalized against the beta-actin house-keeping gene. The dotted line depicts 1.5-fold down- or up-regulation.

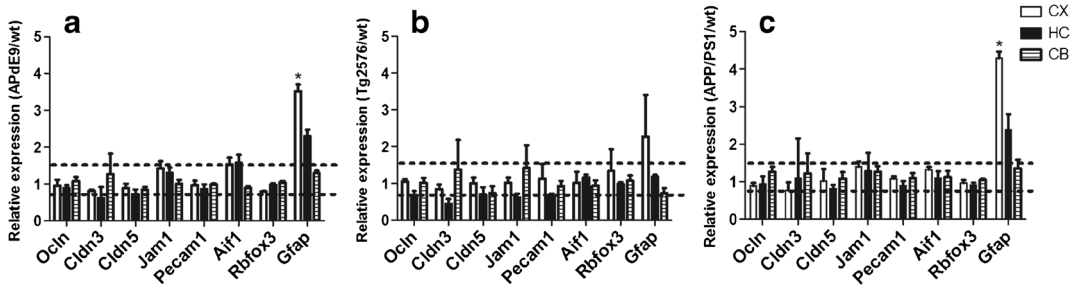

Fig. 3 Gene expression of tight junctions-associated proteins and cell markers in CX, HC and CB of male APdE9 (**a**), female Tg2576 (**b**) and female APP/PS1 (**c**) AD models expressed as relative to wt control mice (AD/wt) (mean ± sd, n = 3–5). The gene expression was normalized against the beta-actin house-keeping gene. The dotted line depicts 1.5-fold down- or up-regulation. *indicates significant difference between AD and wt ($p < 0.05$).

2-fold differences were observed for 20 genes. Only Slco1c1 was equally expressed in all three brain regions. Ocln expression was 5–7 -fold higher in CB than in CX, whereas in CX, the expression of Slc22a3 was ≥5-fold higher than in CB and HC. Interestingly, the expression of Abcc1, Slc7a5, Slc22a5, Slc47a1, Cldn5 and Jam1 was higher (>2-fold) in CB than in CX.

The differences between brain regions were rather similar among all three wt control strains. Since only minor differences were detected between AD and wt mice, these results are mostly comparable also in AD mice models.

Gene and Protein Expression Profile in Brain Microvessel Enriched Fraction of APdE9 Mice

The expression of 35 genes was studied in enriched fraction of microvessels isolated from the cortices of 5–12 weeks old APdE9 mice and age-matched controls. In the case of 11 genes, there was a more than 2-fold difference in the expression level between AD and wt (Table II). Only one gene, Slc2a1, was upregulated by 2-fold in AD; for 10 genes, the AD/wt ratio was <0.5. For the endothelial markers Pecam1 and Cdh5, the ratio was in the range 0.31–0.36. Efflux transporters Abcb1a, Abcc4 and Abcg2

Table I Comparison of gene expression between brain regions in three wt strains (healthy control of each AD mice model i.e. male APdE9, female Tg2576 and female APP/PS1)

	HC/CX APdE9	HC/CX Tg2576	HC/CX APP/PS1	CB/CX APdE9	CB/CX Tg2576	CB/CX APP/PS1	CB/HC APdE9	CB/HC Tg2576	CB/HC APP/PS1
Abcb1a	0.88 ± 0.22	0.86 ± 0.20	0.73 ± 0.15	1.72 ± 0.14	1.67 ± 0.29	1.74 ± 0.10	1.94 ± 0.16	1.95 ± 0.34	2.37 ± 0.13
Abcb1b	1.05 ± 0.20	0.91 ± 0.18	1.13 ± 0.19	0.78 ± 0.11	0.48 ± 0.12*	0.69 ± 0.07	0.75 ± 0.11	0.53 ± 0.13	0.61 ± 0.06
Abcc1	0.95 ± 0.05	0.81 ± 0.18	0.81 ± 0.01	2.37 ± 0.46	2.16 ± 0.22	2.3 ± 0.18	2.5 ± 0.48	2.65 ± 0.27	2.86 ± 0.22
Abcc2	1.12 ± 0.66	0.36 ± 0.16	0.50 ± 0.17	1.15 ± 0.84	0.52 ± 0.59	0.63 ± 0.58	1.03 ± 0.75	1.46 ± 1.65	1.26 ± 1.16
Abcc3	0.90 ± 0.09	0.63 ± 0.13	0.76 ± 0.04	0.61 ± 0.06	0.47 ± 0.27	0.65 ± 0.05	0.68 ± 0.07	0.74 ± 0.43	0.85 ± 0.06
Abcc4	1.13 ± 0.13	0.97 ± 0.21	0.94 ± 0.09	1.97 ± 0.05	1.69 ± 0.31	1.93 ± 0.27	1.75 ± 0.04	1.75 ± 0.32	2.06 ± 0.29
Abcc5	0.68 ± 0.06	0.72 ± 0.05	0.74 ± 0.05	1.37 ± 0.15	1.60 ± 0.21	1.46 ± 0.05	2.01 ± 0.23	2.22 ± 0.30	1.97 ± 0.06
Abcg2	0.87 ± 0.15	0.81 ± 0.2	0.89 ± 0.09	1.31 ± 0.12	1.09 ± 0.17	1.35 ± 0.27	1.52 ± 0.14	1.35 ± 0.21	1.51 ± 0.30
Slc7a5	0.85 ± 0.15	0.79 ± 0.17	0.78 ± 0.09	2.21 ± 0.17	2.01 ± 0.41	2.05 ± 0.16	2.58 ± 0.20	2.55 ± 0.52	2.64 ± 0.21
Slc15a2	0.93 ± 0.08	0.96 ± 0.31	1.09 ± 0.18	1.98 ± 0.10	1.66 ± 0.83	**5.54 ± 0.82**	2.14 ± 0.11	1.74 ± 0.86	**5.09 ± 0.75**
Slc22a2	1.60 ± 1.09	1.80 ± 1.26	0.97 ± 0.41	1.01 ± 0.26	0.71 ± 0.30	0.88 ± 0.16	0.63 ± 0.16	0.40 ± 0.17	0.90 ± 0.17
Slc22a3	**0.15 ± 0.09**	**0.19 ± 0.05**	**0.12 ± 0.05**	**0.18 ± 0.16**	**0.11 ± 0.01**	**0.06 ± 0.05***	1.21 ± 1.06	0.61 ± 0.07	0.52 ± 0.40
Slc22a5	0.91 ± 0.11	1.14 ± 0.23	1.00 ± 0.11	2.09 ± 0.16	2.46 ± 0.50	2.27 ± 0.20	2.29 ± 0.18	2.16 ± 0.44	2.28 ± 0.20
Slc22a8	1.54 ± 0.78	1.27 ± 0.69	0.92 ± 0.46	1.92 ± 0.30	1.77 ± 0.20	1.20 ± 0.13	1.24 ± 0.19	1.40 ± 0.15	1.30 ± 0.14
Slc47a1	0.90 ± 0.77	1.29 ± 0.79	0.85 ± 0.64	2.70 ± 0.84	2.34 ± 1.28	2.10 ± 0.30	3.00 ± 0.94	1.82 ± 1.00	2.48 ± 0.36
Slco1a4	1.12 ± 0.17	0.95 ± 0.43	0.92 ± 0.12	2.09 ± 0.10	1.48 ± 0.36	1.95 ± 0.13	1.86 ± 0.09	1.55 ± 0.38	2.12 ± 0.14
Slco2b1	0.93 ± 0.08	0.82 ± 0.19	0.93 ± 0.18	0.89 ± 0.13	0.45 ± 0.19	1.00 ± 0.05	0.96 ± 0.14	0.55 ± 0.23	1.07 ± 0.05
Slco1c1	0.89 ± 0.16	0.78 ± 0.11	0.83 ± 0.09	1.17 ± 0.21	1.14 ± 0.12	1.08 ± 0.19	1.33 ± 0.23	1.45 ± 0.29	1.30 ± 0.23
Ocln	1.76 ± 0.15	2.55 ± 0.62	1.74 ± 0.15	**5.64 ± 0.16**	**7.25 ± 0.75***	**5.37 ± 0.40**	3.20 ± 0.09	2.84 ± 0.30	3.09 ± 0.23
Cldn3	1.30 ± 1.04	1.87 ± 1.94	1.09 ± 0.16	1.49 ± 0.80	0.89 ± 0.50	1.39 ± 0.94	1.14 ± 0.62	0.47 ± 0.27	1.28 ± 0.87
Cldn5	1.24 ± 0.25	1.14 ± 0.30	0.88 ± 0.33	1.88 ± 0.17	2.12 ± 0.84	1.43 ± 0.28	1.51 ± 0.13	1.86 ± 0.74	1.62 ± 0.32
Jam1	1.05 ± 0.18	1.30 ± 0.96	0.99 ± 0.27	2.38 ± 0.25*	3.78 ± 1.54	1.65 ± 0.29	2.27 ± 0.24	2.91 ± 1.19	1.67 ± 0.30
Pecam1	1.11 ± 0.29	1.06 ± 0.35	0.99 ± 0.27	1.86 ± 0.09	1.44 ± 0.44	1.73 ± 0.17	1.67 ± 0.08	1.36 ± 0.42	1.74 ± 0.17
Aif1	0.76 ± 0.08	0.72 ± 0.14	0.84 ± 0.11	0.80 ± 0.14	0.53 ± 0.18	0.51 ± 0.02	1.06 ± 0.18	0.74 ± 0.25	0.60 ± 0.02
Rbfox3	0.63 ± 0.08	0.73 ± 0.02	0.75 ± 0.02	1.59 ± 0.30	2.18 ± 0.16	2.09 ± 0.23	2.54 ± 0.48	2.97 ± 0.22	2.80 ± 0.30
Gfap	2.18 ± 0.29	2.23 ± 0.50*	2.38 ± 0.25	1.68 ± 0.16	1.85 ± 0.22	2.67 ± 0.45	0.77 ± 0.07	0.83 ± 0.10	1.12 ± 0.19

Results are expressed HC/CX, CB/CX OR CB/HC ratio (mean ± sd, n = 3–5). Yellow color indicates ≥1.5-fold and green color ≥2-fold differences between brain regions. * = $p < 0.05$

had 73%, 60% and 55% lower expression levels, respectively, in AD than in wt. A similar trend was observed in case of the expression of the influx transporters Slc22a8 (55%) and Slco1a4 (61%), beta-amyloid peptide receptor Ager (Rage) (65%) and tight junction-associated genes occludin (60%) and claudin 5 (64%).

Results were normalized against beta-actin, which showed stable expression between AD and wt samples. Since the amount of RNA was limited, the replicate measurements were focused on genes with moderate or high expression and/or where a difference between AD and wt was detected in the first measurement.

The microvessel enriched fraction was used also to study the protein expression of the main receptors for amyloid-beta peptide, Rage and Lrp1, with the efflux transporters Mdr1 and Mrp4 showing lower gene expression in AD than in wt mice. According to the results of immunoblotting, the expression of these proteins did not differ significantly (≤ 1.5-fold) between AD and wt samples (Fig. 4).

Distribution of Methotrexate into Brain in APdE9 Mice

To assess the effect of AD pathology on efflux transporter function *in vivo*, methotrexate was selected as a model drug for the

Table II Comparison of Gene Expression Levels between Brain Microvessels Isolated from Cortices of Female AD Mice (APdE9) and their wt Controls

ATP-binding cassette (ABC) transporters		
Gene	Protein	Ratio of AD/wt[a]
Abcb1a	Multidrug resistance protein 1a (Mdr1a)	0.258–0.283
Abcb1b	Multidrug resistance protein 1b (Mdr1b)	0.537
Abcc1	Multidrug resistance-associated protein 1 (Mrp1)	0.758
Abcc2	Multidrug resistance-associated protein 2 (Mrp2)	0.677
Abcc3	Multidrug resistance-associated protein 3 (Mrp3)	1.011
Abcc4	Multidrug resistance-associated protein 4 (Mrp4)	0.3971–0.3973
Abcc5	Multidrug resistance-associated protein 5 (Mrp5)	0.588–0.668
Abcg2	Breast cancer resistance protein (Bcrp)	0.436–0.457
Solute carriers (SLCs)		
Slc2a1	Glucose transporter 1 (Glut1)	1.803–2.230
Slc5a7	High affinity choline transporter 1 (Cht1)	1.173–1.653
Slc7a5	L-type amino acid transporter 1 (Lat1)	0.696–0.943
Slc15a2	Peptide transporter 2 (Pept2)	0.766–0.913
Slc16a1	Monocarboxylate transporter 1 (Mct1)	0.620–0.657
Slc22a2	Organic cation transporter 2 (Oct2)	1.161
Slc22a3	Organic cation transporter 3 (Oct3)	0.990
Slc22a5	Organic cation/carnitine transporter 2 (Octn2)	0.626
Slc22a8	Organic anion transporter 3 (Oat3)	0.414–0.495
Slc29a1	Equilibrative transporter 1 (Ent1)	0.941–1.03
Slc47a1	Multidrug and toxin extrusion protein 1 (Mate1)	0.543
Slco1a4	Organic anion transporting polypeptide 1a4 (Oatp1a4)	0.369–0.405
Slco2b1	Organic anion transporting polypeptide 2b1 (Oatp2b1)	0.714–0.726
Slco1c1	Organic anion transporting polypeptide 1c1 (Oatp1c1)	0.525–0.563
Transport of beta-amyloid		
	Full name	
Lrp1	Low density lipoprotein receptor-related protein 1	0.960–0.964
Ager	Advanced glycation end product-specific receptor (Rage)	0.300–0.400
Tight junction-associated proteins		
Odn	Occludin	0.362–0.431
Cldn1	Claudin1	1.079–1.334
Cldn3	Claudin 3	1.052
Cldn5	Claudin 5	0.308–0.410
Tjp1	Tight junction protein ZO-1	0.555–0.646
F11r	Junctional adhesion molecule A (Jam-A)	0.591–0.666
Cell markers		
	Full name/Cell type	
Pecam1	Platelet/endothelial cell adhesion molecule 1/Endothelial	0.324–0.363
Cdh5	Cadherin-5/Endothelial	0.306–0.354
Aif1	Allograft inflammatory factor 1/Microglial	0.826–0.898
Gfap	Glial fibrillary acidic protein/Astrocytic	1.07–1.09
Rbfox3	RNA binding protein, fox-1 homolog (*C. elegans*) 3/Neuronal	1.243

[a] When results are expressed as range, two replicate samples were used. Otherwise the results are based on one sample of isolated microvessels. Each sample is a pool from brain microvessels of 5 mice

brain microdialysis studies since it has been previously shown to be effluxed by both Mrp4 and Bcrp in a similar study conducted in Mrp4 and Bcrp knock-out mice (23). Unbound extracellular methotrexate levels in hippocampus were 9-fold higher in APdE9 mouse than the corresponding values in wt in the 20 min fraction after drug administration (Fig. 5), but the difference diminished later. The brain methotrexate exposure ($AUC_{0-\infty}$) was 2.7-fold higher in APdE9 than in wt ($p = 0.013$) mice and the difference was even greater, 2.9-fold ($p = 0.006$), within the first 60 min (AUC_{0-60}) (Table III). Total plasma concentration was measured after intravenous injection of methotrexate from separate mice (wt $n = 6$ and APdE9 $n = 5–6$, 17 months). The plasma concentrations at 10, 30 and 60 min were 52.7 ± 7, 14.0 ± 7.2 and 5.9 ± 1.1 μg/ml (mean ± sd) in APdE9 and 58.4 ± 16, 14.1 ± 4.5 and 6.6 ± 2.6 μg/ml in wt mice, respectively.

DISCUSSION

Transporters and tight junctions of the BBB are crucial for the maintenance of brain homeostasis. Neurodegenerative diseases, such as AD, alter the function of the BBB and are therefore likely to change drug distribution into the brain (24). In this study, the expression of Abc and Slc transporters relevant in pharmacokinetics and tight junction-associated proteins in the brains of three AD mouse models, APdE9, Tg2576 and APP/PS1 were investigated. We focused on genes that are known to be expressed in brain/BBB. Brain samples were dissected from >12 months old animals having clear pathological signs of the disease in their brain i.e. amyloid beta plaques and gliosis. We used APP and APP/PS1 mutant mouse lines considered to be AD models of Aβ pathology rather than AD models fully addressing the clinical presentation of AD. The expression levels of the studied genes in AD models were close to their healthy age-matched controls and the observed differences were minor

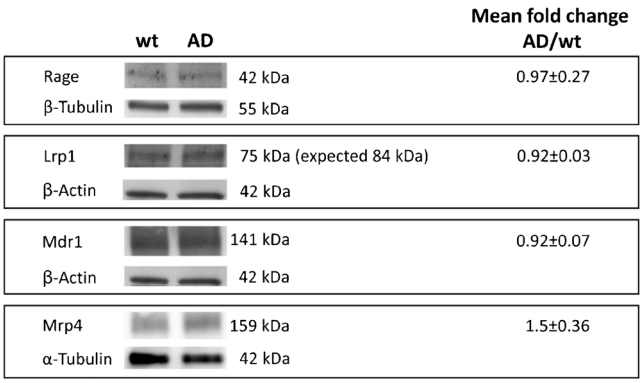

Fig. 4 Expression of Rage, Lrp1, Mdr1 and Mrp4 proteins in microvessel enriched fraction isolated from cortices of female APdE9 (AD) and wt mouse and detected by Western blotting. For Rage, Lrp1 and Abcb1 40 μg of total protein were used, the corresponding value for Mrp4 was 5 μg. Mean fold change ± SEM (AD/wt) was calculated based on three replicate blots

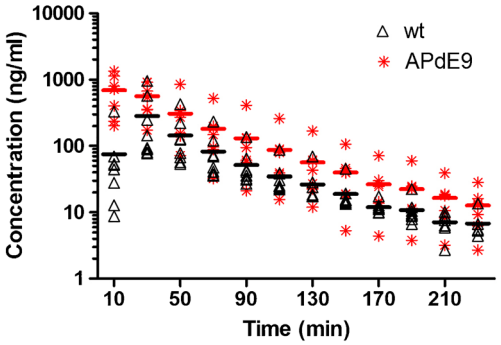

Fig. 5 Unbound extracellular methotrexate levels in the hippocampus of male APdE9 mice (AD) ($n = 7$) and wt controls ($n = 8$) after i.v. injection at 50 mg/kg. Microdialysis samples were collected as 20 min fractions. LLOQ was 0.05 ng/ml

(mostly less than 1.5-fold change) with the exception of the astrocyte cell marker, Gfap. This was expected since upregulation of Gfap due to an increase in the numbers of reactive astrocytes is an early and common sign in various models of neurodegeneration and brain diseases, and is also observed in transgenic AD mice (25). Furthermore, the expression of the microglial activation marker, Aif1, was elevated (about 1.5-fold) in APdE9 mice in line with extensive data revealing neuroinflammation as a characteristic of AD.

Comparison of gene expression of transporters and tight junction-associated proteins between brain regions showed more than 2-fold differences for 21 genes in wt mice. For 14 genes, a higher expression level was observed in CB in comparison to CX or HC. We detected a > 5-fold difference between brain regions in gene expression of organic cation transporter Slc22a3 and the tight junction-associated protein, occludin. Such large differences in gene expression should reflect protein expression and functionality. In the literature, the data regarding regional variability of brain drug transporters is sparse and scattered. The highest Mdr1 activity has been proposed for CB by a combinatory mapping approach and PET studies in rats (26,27). These observations are in accordance with our data as Abcb1a is the major form in brain. However, in another study, Mdr1 mediated efflux activity of loperamide was highest in cerebral CX and midbrain regions when assessed by *in situ* brain perfusion in mice (28). Kannan *et al.* stated that there was equal BCRP density

Table III Brain Exposure to Methotrexate in Male APdE9 Mice (AD) and their wt Controls After i.v. Injection at 50 mg/kg. AUC Calculated from Whole Concentration-Time Curve ($AUC_{0-\infty}$) and First 60 min (AUC_{0-60}) are Presented (mean ± SEM, n = 7–8)

	AD	wt control
$AUC_{0-\infty}$ (ng x min/ml)	40178 ± 7587*	15107 ± 4765
AUC_{0-60} (ng x min/ml)	27485 ± 4167**	9507 ± 3604

*$p < 0.05$ *vs.* wt control value

**$p < 0.01$ *vs.* wt control value

between brain regions, which is also in line with our results (13). The high regional variability in transporter expression may perhaps be explained by the higher capillary density in certain brain region or the variation in the relative amount of each cell type. Previously, brain capillary density has been determined with the vascular volume marker, inulin, with a 3.7-fold difference being observed between brain regions (28). This high variation between brain areas can affect the regional distribution of drugs in brain, but more information about transporter expression at the cell type level will be needed to estimate the effect of regional variability on brain pharmacokinetics and access of drugs to their target site.

The endothelial cells of the BBB and tight junctions expressed between these cells form the physical barrier for brain distribution of drugs. Since the brain microvessels comprise only 0.1% of brain weight and brain tissue contains many cell types (endothelial cells, astrocytes, microglial cells, neurons and pericytes), the alterations in gene and protein expression occurring solely in the microvessel endothelial cells can be interfered by other cell types. Therefore, further studies to reveal AD-induced changes in BBB protein expression were conducted by using brain microvessels isolated from APdE9 mice. The isolation of a microvessel enriched fraction is feasible only in young mice (≤12 weeks), whose brain pathology of AD is still developing. The normalized expressions of endothelial markers, Pecam1 and Cdh5, were about 3-fold lower in APdeE9 compared to their healthy control mice, suggesting that APP and PSEN1 mutations may considerably affect the brain vasculature already during development or in young adulthood. Both increased and decreased vascular densities have been reported in AD (29).

The gene expression of Abcb1a was downregulated in the microvessel enriched fraction which is in line with the earlier reports from AD patients and animal models (8,10). Furthermore, Abcc4 and Abcg2 were downregulated. In order to assess the effect of AD pathology on efflux transporter function, MTX was selected as a model drug, because it has been previously demonstrated to cross the BBB via Mrp4 and Bcrp in a brain microdialysis study conducted in Mrp4 and Bcrp knock-out mice (23). Methotrexate is also a substrate for MDR1, OAT and OATP transporters (30–34). Since Abcb1a (Mdr1a), Slac22a8 (Oat3) and Slco1a4 (Oatp1a4) were also downregulated in the microvessel enriched fraction, it is possible that these transporters participate in the distribution of methotrexate into the brain. As far as we are aware, this is the first study where AD-induced changes in brain unbound extracellular drug concentrations have been studied by pharmacokinetic microdialysis in the context of transporter function.

Brain microdialysis revealed that methotrexate gained faster access into the brain in 16–18 months old APdE9 mice after drug administration but the difference *vs.* wt controls diminished later. This finding may reflect alterations in the active transport in BBB or otherwise compromised BBB. Identification of functionally altered transporter(s) is challenging due to overlapping substrate specificities and would require experiments with inhibitors. The consequences of BBB disruption, even when local or transient, can be harmful for the homeostasis of brain. Aβ has been reported to compromise BBB tight junction proteins and thus BBB integrity in human amyloid precursor protein transgenic mice (35) and human apoE4 transgenic mice (36). Generally, in tumor-bearing rats, a compromised BBB has been shown to increase brain extracellular MTX levels shortly after drug administration (37). However, Bien-Ly *et al.* (2015) reported recently that brain access of antibodies and radiotracers was not significantly altered in AD mouse models (38). Cheng *et al.* (2010) also reported that brain penetration of some small-molecule drugs was unaltered in AD-related animal models and Mehta *et al.* (2013) even found decreased brain uptake of transcellular permeability markers (diazepam and propranolol) in the 3xTg model possibly due to thickening of the basement membrane (16,39). Furthermore, imaging studies with AD patients have not found convincing evidence that AD alone, without a vascular component, causes BBB disruption (2). These discrepancies both in experimental models of AD and patients may partly be due to variation in the degree of AD pathology and the characteristics of the model drugs. Accumulation of Aβ plaques within the extracellular space, severe shrinkage of cerebral cortex and hippocampus, and an increase in the size of the ventricles in AD brains may affect the distribution of drugs in brain tissue. For a hydrophilic drug like methotrexate ($LogD_{pH7.4}$–5.22, Chemspider, predicted using ACD/Labs), a smaller volume of extracellular fluid can lead to higher initial drug concentration in AD mice after a single systemic dose.

No significant differences were detected between <3 month old APdE9 mice and their controls at the protein level in the expression of Mdr1, Mrp4, Rage and Lrp1 in the microvessel enriched fraction. Earlier, Hartz *et al.* (2010) demonstrated that Mdr1 expression was decreased by approximately 60% and efflux of Mdr1 substrate NBD-CSA was reduced by 70% in brain capillaries of Tg2576 mice (8). Recently, Do *et al.* (2016) stated that Abcb1 and Abcg2 expressions in the brain capillary fraction of another AD model, 3xTg-AD were upregulated by 1.7-fold at 18 months of age, although younger mice (3 and 6 months) did not display significant changes (17). With the same AD model, Mehta *et al.* reported that cortical or hippocampal uptake of three Mdr1 substrates, digoxin, loperamide and verapamil, was not significantly altered in 18–20 month old 3xTg-AD mice (16). However, Mdr1 expression showed variability between replicates, ranging from a 42% reduction to no difference in 3xTg-AD compared to wt controls. These results demonstrate that alterations in efflux proteins, induced by AD-causing mutations, are minor in animal models but comparable to those encountered in human studies.

The expression level of transporters affects the maximum velocity of transport (V_{max}) and therefore, it can be assumed to reflect in transport function. A decrease in the transporter

expression is comparable to the inhibition kinetics of active transport, where the degree of inhibition increases with inhibitor concentration (40). Should efflux transporter expression decrease by 50%, this would cause at maximum a 2-fold increase in the steady state drug concentration in the brain, assuming that the drug passes through the BBB exclusively via this specific transporter. Similarly, a 67% decline in expression would cause at maximum a 3-fold and an 80% decline would evoke a maximum of a 5-fold increase in brain drug concentration at steady state. If we consider the clinical relevance of alterations detected in AD patients, mostly 2-fold or smaller alterations for MDR1 have been observed. For instance, when the activity of MDR1 was studied with PET imaging, the binding potential of verapamil was found to be modestly increased in AD patients (2.18 ± 0.25) compared to healthy controls (1.77 ± 0.41) (14). In addition, the expression of MDR1 was 25% lower in the blood vessels of AD patients than age–matched controls when hippocampal sections were studied by immunofluorescence (10). Accordingly, when Kannan *et al.* recently studied transporter density in the vascular space, they found that MDR1 global density was 53% lower in the temporal CX of AD patients as compared to controls, and in capillaries near to Aβ deposits, the MDR1 density was locally decreased by 35% (13). Our present results with AD models are in line with these observations. Therefore, in order that a detected approximately 2-fold change in expression level should be clinically significant, the drug should have an extremely narrow therapeutic level and adverse effects in brain should be the dose-limiting factor, an extremely rare situation for clinically used drugs (40). It should be kept in mind that in addition to the expression level, transporter functionality is also dependent on other factors such as post-translational modifications and changes in membrane composition, which may change in Alzheimer's disease and affect binding affinity and transport activity. Furthermore, binding to plasma proteins is an important factor influencing drug distribution into the brain since only unbound drug is able to cross the endothelial cell barrier. Disease states can change the plasma protein binding, but thus far, no significant changes in plasma protein content have been observed in AD patients. In addition to the influence of disease, other factors such as age and sex may affect transporter expression (41, 42). However, in this study, we used age-matched controls of the same gender in order to assess the effect of AD on drug transporters.

In conclusion, transporter expression varied significantly between brain areas in both transgenic AD mice and wt mice. However, disease-induced alterations in transporter expression were low in all studied transgenic AD mouse models, which accords with the current knowledge on disease-induced changes in AD patients. Decreased expression of some transporters and tight junction-associated proteins in brain microvessel fraction of APdE9 mice as well as more rapid brain access of MTX in APdE9 mice indicate that AD pathology may contribute to the BBB functionality to some extent.

ACKNOWLEDGMENTS AND DISCLOSURES

This study was funded by Academy of Finland (Grant number 257386). Finnish Cultural Foundation is also acknowledged for financial support. KMK and TM acknowledges the funding from the Academy of Finland and Sigrid Juselius Foundation. We thank Dr. Aaro Jalkanen for advice in designing microdialysis experiment, Prof. Seppo Auriola for consultation in LC-MS/MS analysis and Lecturer Veli-Pekka Ranta for advice regarding pharmacokinetics. Mrs. Jaana Leskinen, Mrs. Leena Pietilä and Mrs. Lea Pirskanen are acknowledged for technical assistance. The authors declare that they have no conflict of interest. All applicable international, national and institutional guidelines for the care and use of animals were followed. All procedures performed in studies involving animals were in accordance with the ethical standards of the University of Eastern Finland or practice at which the studies were conducted. This article does not contain any studies with human participants performed by any of the authors.

REFERENCES

1. Ballard C, Gauthier S, Corbett A, Brayne C, Aarsland D, Jones E. Alzheimer's disease. Lancet. 2011;377(9770):1019–31.
2. Erickson MA, Banks WA. Blood-brain barrier dysfunction as a cause and consequence of Alzheimer's disease. J Cereb Blood Flow Metab. 2013;33(10):1500–13.
3. Stieger B, Gao B. Drug transporters in the central nervous system. Clin Pharmacokinet. 2015;54(3):225–42.
4. Uchida Y, Ohtsuki S, Katsukura Y, Ikeda C, Suzuki T, Kamiie J, et al. Quantitative targeted absolute proteomics of human blood-brain barrier transporters and receptors. J Neurochem. 2011;117(2):333–45.
5. Agarwal S, Uchida Y, Mittapalli RK, Sane R, Terasaki T, Elmquist WF. Quantitative proteomics of transporter expression in brain capillary endothelial cells isolated from P-glycoprotein (P-gp), breast cancer resistance protein (Bcrp), and P-gp/Bcrp knockout mice. Drug Metab Dispos. 2012;40(6):1164–9.
6. Geier EG, Chen EC, Webb A, Papp AC, Yee SW, Sadee W, et al. Profiling solute carrier transporters in the human blood-brain barrier. Clin Pharmacol Ther. 2013;94(6):636–9.
7. Nies AT, Jedlitschky G, Konig J, Herold-Mende C, Steiner HH, Schmitt HP, et al. Expression and immunolocalization of the multidrug resistance proteins, MRP1-MRP6 (ABCC1-ABCC6), in human brain. Neuroscience. 2004;129(2):349–60.
8. Hartz AM, Miller DS, Bauer B. Restoring blood-brain barrier P-glycoprotein reduces brain amyloid-beta in a mouse model of Alzheimer's disease. Mol Pharmacol. 2010;77(5):715–23.
9. Vogelgesang S, Cascorbi I, Schroeder E, Pahnke J, Kroemer HK, Siegmund W, et al. Deposition of Alzheimer's beta-amyloid is inversely correlated with P-glycoprotein expression in the brains of elderly non-demented humans. Pharmacogenetics. 2002;12(7):535–41.

10. Wijesuriya HC, Bullock JY, Faull RL, Hladky SB, Barrand MA. ABC efflux transporters in brain vasculature of Alzheimer's subjects. Brain Res. 2010;1358:228–38.
11. Jeynes B, Provias J. An investigation into the role of P-glycoprotein in Alzheimer's disease lesion pathogenesis. Neurosci Lett. 2011;487(3):389–93.
12. Carrano A, Snkhchyan H, Kooij G, van der Pol S, van Horssen J, Veerhuis R, et al. ATP-binding cassette transporters P-glycoprotein and breast cancer related protein are reduced in capillary cerebral amyloid angiopathy. Neurobiol Aging. 2014;35(3):565–75.
13. Kannan P, Schain M, Kretzschmar WW, Weidner L, Mitsios N, Gulyas B, et al. An automated method measures variability in P-glycoprotein and ABCG2 densities across brain regions and brain matter. J Cereb Blood Flow Metab. 2016;01:271678X16660984.
14. van Assema DM, Lubberink M, Bauer M, van der Flier WM, Schuit RC, Windhorst AD, et al. Blood-brain barrier P-glycoprotein function in Alzheimer's disease. Brain. 2012;135(Pt 1):181–9.
15. Xiong H, Callaghan D, Jones A, Bai J, Rasquinha I, Smith C, et al. ABCG2 is upregulated in Alzheimer's brain with cerebral amyloid angiopathy and may act as a gatekeeper at the blood-brain barrier for Abeta(1–40) peptides. J Neurosci. 2009;29(17):5463–75.
16. Mehta DC, Short JL, Nicolazzo JA. Altered brain uptake of therapeutics in a triple transgenic mouse model of Alzheimer's disease. Pharm Res. 2013;30(11):2868–79.
17. Do TM, Dodacki A, Alata W, Calon F, Nicolic S, Scherrmann JM, et al. Age-dependent regulation of the blood-brain barrier influx/efflux equilibrium of amyloid-beta peptide in a mouse model of Alzheimer's disease (3xTg-AD). J Alzheimers Dis. 2016;49(2):287–300.
18. Jankowsky JL, Fadale DJ, Anderson J, Xu GM, Gonzales V, Jenkins NA, et al. Mutant presenilins specifically elevate the levels of the 42 residue beta-amyloid peptide in vivo: evidence for augmentation of a 42-specific gamma secretase. Hum Mol Genet. 2004;13(2):159–70.
19. Jankowsky JL, Slunt HH, Ratovitski T, Jenkins NA, Copeland NG, Borchelt DR. Co-expression of multiple transgenes in mouse CNS: a comparison of strategies. Biomol Eng. 2001;17(6):157–65.
20. Hsiao K, Chapman P, Nilsen S, Eckman C, Harigaya Y, Younkin S, et al. Correlative memory deficits, Abeta elevation, and amyloid plaques in transgenic mice. Science. 1996;274(5284):99–102.
21. Coisne C, Dehouck L, Faveeuw C, Delplace Y, Miller F, Landry C, et al. Mouse syngenic in vitro blood-brain barrier model: a new tool to examine inflammatory events in cerebral endothelium. Lab Investig. 2005;85(6):734–46.
22. Muller PY, Janovjak H, Miserez AR, Dobbie Z. Processing of gene expression data generated by quantitative real-time RT-PCR. BioTechniques. 2002;32(6):1372. -4, 1376, 1378-9
23. Sane R, Wu SP, Zhang R, Gallo JM. The effect of ABCG2 and ABCC4 on the pharmacokinetics of methotrexate in the brain. Drug Metab Dispos. 2014;42(4):537–40.
24. Pahnke J, Langer O, Krohn M. Alzheimer's and ABC transporters–new opportunities for diagnostics and treatment. Neurobiol Dis. 2014;72(Pt A):54–60.
25. Middeldorp J, Hol EM. GFAP in health and disease. Prog Neurobiol. 2011;93(3):421–43.
26. Loryan I, Melander E, Svensson M, Payan M, Konig F, Jansson B, et al. In-depth neuropharmacokinetic analysis of antipsychotics based on a novel approach to estimate unbound target-site concentration in CNS regions: link to spatial receptor occupancy. Mol Psychiatry. 2016;21(11):1527–36.
27. Kuntner C, Bankstahl JP, Bankstahl M, Stanek J, Wanek T, Stundner G, et al. Dose-response assessment of tariquidar and elacridar and regional quantification of P-glycoprotein inhibition at the rat blood-brain barrier using (R)-[(11)C]verapamil PET. Eur J Nucl Med Mol Imaging. 2010;37(5):942–53.
28. Zhao R, Pollack GM. Regional differences in capillary density, perfusion rate, and P-glycoprotein activity: a quantitative analysis of regional drug exposure in the brain. Biochem Pharmacol. 2009;78(8):1052–9.
29. Brown WR, Thore CR. Review: cerebral microvascular pathology in ageing and neurodegeneration. Neuropathol Appl Neurobiol. 2011;37(1):56–74.
30. van de Steeg E, van der Kruijssen CM, Wagenaar E, Burggraaff JE, Mesman E, Kenworthy KE, et al. Methotrexate pharmacokinetics in transgenic mice with liver-specific expression of human organic anion-transporting polypeptide 1B1 (SLCO1B1). Drug Metab Dispos. 2009;37(2):277–81.
31. Badagnani I, Castro RA, Taylor TR, Brett CM, Huang CC, Stryke D, et al. Interaction of methotrexate with organic-anion transporting polypeptide 1A2 and its genetic variants. J Pharmacol Exp Ther. 2006;318(2):521–9.
32. Zhu Y, Meng Q, Wang C, Liu Q, Huo X, Zhang A, et al. Methotrexate-bestatin interaction: involvement of P-glycoprotein and organic anion transporters in rats. Int J Pharm. 2014;465(1–2):368–77.
33. Kanamitsu K, Kusuhara H, Schuetz JD, Takeuchi K, Sugiyama Y. Investigation of the importance of multidrug resistance-associated protein 4 (Mrp4/Abcc4) in the active efflux of anionic drugs across the blood-brain barrier. J Pharm Sci. 2017;106(9):2566–75.
34. Takeda M, Khamdang S, Narikawa S, Kimura H, Hosoyamada M, Cha SH, et al. Characterization of methotrexate transport and its drug interactions with human organic anion transporters. J Pharmacol Exp Ther. 2002;302(2):666–71.
35. Hartz AM, Bauer B, Soldner EL, Wolf A, Boy S, Backhaus R, et al. Amyloid-beta contributes to blood-brain barrier leakage in transgenic human amyloid precursor protein mice and in humans with cerebral amyloid angiopathy. Stroke. 2012;43(2):514–23.
36. Bell RD, Winkler EA, Singh I, Sagare AP, Deane R, Wu Z, et al. Apolipoprotein E controls cerebrovascular integrity via cyclophilin A. Nature. 2012;485(7399):512–6.
37. de Lange EC, de Vries JD, Zurcher C, Danhof M, de Boer AG, Breimer DD. The use of intracerebral microdialysis for the determination of pharmacokinetic profiles of anticancer drugs in tumor-bearing rat brain. Pharm Res. 1995;12(12):1924–31.
38. Bien-Ly N, Boswell CA, Jeet S, Beach TG, Hoyte K, Luk W, et al. Lack of widespread BBB disruption in Alzheimer's disease models: Focus on therapeutic antibodies. Neuron. 2015;88(2):289–97.
39. Cheng Z, Zhang J, Liu H, Li Y, Zhao Y, Yang E. Central nervous system penetration for small molecule therapeutic agents does not increase in multiple sclerosis- and Alzheimer's disease-related animal models despite reported blood-brain barrier disruption. Drug Metab Dispos. 2010;38(8):1355–61.
40. Kalvass JC, Polli JW, Bourdet DL, Feng B, Huang SM, Liu X, et al. Why clinical modulation of efflux transport at the human blood-brain barrier is unlikely: the ITC evidence-based position. Clin Pharmacol Ther. 2013;94(1):80–94.
41. Kelly SD, Harrell CS, Neigh GN. Chronic stress modulates regional cerebral glucose transporter expression in an age-specific and sexually-dimorphic manner. Physiol Behav. 2014;126:39–49.
42. Flores K, Manautou JE, Renfro JL. Gender-specific expression of ATP-binding cassette (Abc) transporters and cytoprotective genes in mouse choroid plexus. Toxicology. 2017;386:84–92.